Research Article

Hanan A. Althobiti, Sami A. Zabin*

New Schiff bases of 2-(quinolin-8-yloxy)acetohydrazide and their Cu(II), and Zn(II) metal complexes: their *in vitro* antimicrobial potentials and *in silico* physicochemical and pharmacokinetics properties

https://doi.org/10.1515/chem-2020-0085
received December 27, 2019; accepted April 18, 2020

Abstract: The purpose of this work was to prepare Schiff base ligands containing quinoline moiety and using them for preparing Cu(II) and Zn(II) complexes. Four bidentate Schiff base ligands (SL_1–SL_4) with quinoline hydrazine scaffold and a series of mononuclear Cu(II) and Zn(II) complexes were successfully prepared and characterized. The *in vitro* antibacterial and antifungal potential experimentation revealed that the ligands exhibited moderate antibacterial activity against the Gram-positive bacterial types and were inactive against the Gram-negative bacteria and the fungus strains. The metal complexes showed some enhancement in the activity against the Gram-positive bacterial strains and were inactive against the Gram-negative bacteria and the fungus strains similar to the parent ligands. The complex $[Cu(SL_1)_2]$ was the most toxic compound against both Gram-positive *S. aureus* and *E. faecalis* bacteria. The *in silico* physicochemical investigation revealed that the ligand SL_4 showed highest *in silico* absorption (82.61%) and the two complexes $[Cu(SL_4)_2]$ and $[Zn(SL_4)_2]$ showed highest *in silico* absorption with 56.23% for both compounds. The *in silico* pharmacokinetics predictions showed that the ligands have high gastrointestinal (GI) absorption and the complexes showed low GI absorption. The ligands showed a good bioavailability score of 0.55 where the complexes showed moderate to poor bioavailability.

Key words: Schiff bases, quinoline hydrazine, metal complexes, antimicrobial, *in silico* predictions

*** Corresponding author: Sami A. Zabin,** Chemistry Department, Faculty of Science, Albaha University, Al-Baha, Saudi Arabia, e-mail: samizabin@gmail.com, szabin@bu.edu.sa, tel: +966 554676466
Hanan A. Althobiti: Chemistry Department, Faculty of Science, Albaha University, Al-Baha, Saudi Arabia

1 Introduction

The chemical compounds containing azomethine group called Schiff bases are an excellent class of ligands and are widely used in coordination chemistry. These chemicals have the ability to react with metal ions producing versatile coordination metal complexes, which have wide applications in different fields [1,2]. It is well established in the literature that the presence of the main functional azomethine group (–CH═N–) in the structure of the Schiff bases is a characteristic feature of these compounds and responsible for their various biological potentials and medicinal actions [3,4].

The Schiff bases containing heterocyclic systems have been a fertile area of research for a long period, and there is a vast literature work on Schiff base complexes comprising heterocyclic structures [5]. The complexes derived from quinoline and quinoline derivatives currently attracted the interest among the Schiff base ligands containing heterocyclic ring. The Schiff bases containing quinoline nucleus have more favored attention mainly due to their potential applications in the medicinal field [6–10].

In view of the facts and the important features of Schiff bases containing quinoline moiety as reported in the literature, we encouraged and focused our investigation to design new ligand compounds with such structures. The suggested Schiff base ligands were derived from 2-(quinolin-8-yloxy)acetohydrazide as a primary amine condensed with different aromatic aldehydes such as salicylaldehyde, *o*-vaniline, 2-hydroxy-1-naphthaldehyde, and 3-pyridinecarbaldehyde. The synthesized ligands were used further to synthesize metal complexes with copper and zinc metal ions. All synthesized compounds were investigated *in vitro* for their antibacterial and antifungal potentials. Moreover, the prepared compounds were subjected to *in silico* physicochemical and pharmacokinetics investigation to predict the absorption, distribution, metabolism, and elimination (ADME) drug-likeness properties.

The targeted compounds were prepared successfully, and their antimicrobial potential was comparatively weak.

2 Materials and methods

2.1 Materials

All starting chemicals and solvents used in this study were of reagent grade, obtained from Sigma-Aldrich, Luba, and BDH Chemical Companies. The primary aromatic amine compound 2-(quinolin-8-yloxy)acetohydrazide was synthesized from 8-hydroxy quinoline in our laboratory following the literature reported method [11,12].

2.2 Instrumentation and physical measurements

For characterization of the prepared ligands and their metal complexes, we used different physical and spectroscopic analysis techniques. The melting points were measured utilizing the electro-thermal IA9100 digital melting point apparatus. The micro-elemental analysis was determined using the Thermo Fisher Scientific CHN/S/O analyzer instrument (Leco Model VTF-900 CHN-S-O 932 version 1.3x USA). Metal percentage in the complexes was determined using Inductively Coupled Plasma Optical Emission Spectrometry (ICP-OES). For this purpose, the instrument used was Thermo Fisher Scientific ICP-7000 plus Series ICP-OS spectrophotometer (USA). Mass spectroscopy was obtained from the Thermo Fisher Scientific-LCQ fleet ion trap mass spectrometer (USA) using the electrospray ionization (ESI) method.

UV-visible absorption spectra measurements were performed on Thermo Fisher Scientific Evolution 300 UV-visible double beam spectrophotometer (USA) using 0.001 M dimethyl sulfoxide (DMSO) solution. FT-IR spectra were obtained in the range 400–4,000 cm^{-1} on Thermo Fisher Scientific Nicolet iS50 FT-IR spectrophotometer (USA) using attenuated total reflection (ATR) method for direct measurement of the IR spectrum for the powder solid samples. ^{1}H and ^{13}C NMR spectra of the ligands and the metal complexes were recorded via Bruker 400 MHz spectrometer (Germany) using DMSO as the solvent at the Faculty of Science, Suhag University, Egypt. The magnetic susceptibilities of complexes were measured by the Gouy method at room temperature using the Sherwood scientific magnetic susceptibility balance (UK) and using distilled water as the calibrant. The measurements were carried out at the Central Laboratory, Faculty of Science, Cairo University, Egypt. Molar conductance of the metal complexes was measured using the Fisher Scientific AP85 Portable Waterproof PH/conductivity meter (Italy). The molar conductance measurements were performed using 0.001 M solutions of the complexes in DMSO at room temperature. Thermal analysis measurements were performed on Shimadzu thermo-analyzer TG-50H (Japan) in a nitrogen atmosphere and rate flow 20.0 mL/min at a heating rate of 10°C/min in the temperature range 25–1,000°C.

2.3 Preparation of 2-(quinolin-8-yloxy) actohydrazide precursor

The main primary amine compound 2-(quinolin-8-yloxy) acetohydrazide (Figure 1) was prepared in two steps following reported method by the reaction of 8-hydroxyquinoline (0.02 mol) with ethyl chloroacetate (0.02 mol) in dry acetone to get ethyl ester of *o*-alkylated 8-hydroxyquinoline and then reacted with hydrazine hydrate (0.04 mol). The yield was 81.3% and the melting point measured 138°C similar to the reported one [11–13].

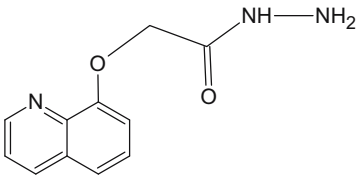

Figure 1: Structure of 2-(quinolin-8-yloxy)acetohydrazide.

2.4 General method for synthesis of the Schiff base ligands (SL_1–SL_4)

The organic Schiff base ligands (SL_1–SL_4) were synthesized according to the standard methods [14]. The primary amine 2-(quinolin-8-yloxy)acetohydrazide (0.01 mol) was dissolved in ethanol and mixed with the stoichiometric quantity (0.01 mol) of the aldehydic compound dissolved in ethanol with continuous stirring using a hot-stage magnetic stirrer and refluxing the mixture for a proper

time of 1–2 h. Completion of reactions was checked with thin layer chromatography (TLC), and the obtained products after cooling to room temperature were filtered, dried, and finally purified by recrystallization. Physical characteristics, elemental analysis, and percentage of yield for each prepared Schiff base are detailed in the following sections.

2.4.1 Synthesis of *N'*-[(*E*)-(2-hydroxyphenyl) methylidene]-2-[(quinolin-8-yl)oxy] acetohydrazide (SL_1)

For the preparation of SL_1 (Figure 2), a mixture of 2-(quinolin-8-yloxy)acetohydrazide 0.01 mol was reacted with 0.01 mol salicylaldehyde in ethanol with stirring using a hot-stage magnetic stirrer and refluxed for nearly 2 hours. The whitish-yellow solid precipitate was filtered, washed with ethanol, dried, and finally recrystallized in hot ethanol. The yield obtained was 82%, and the measured melting point was 132°C. Elemental analysis for $C_{18}H_{15}N_3O_3$: cal. (found), %C 67.34 (67.02), %H 4.67 (4.77), %N 13.08 (13.36), and %O 14.95 (14.63).

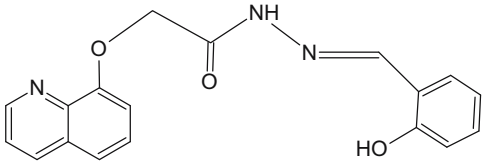

Figure 2: Structure of SL_1 ligand.

2.4.2 Synthesis of *N'*-[(*E*)-(2-hydroxy-3-methoxyphenyl) methylidene]-2-[(quinolin-8-yl) oxy]acetohydrazide (SL_2)

For the preparation of SL_2 (Figure 3), 0.01 mol of 2-(quinolin-8-yloxy)acetohydrazide was mixed with 0.01 mol *o*-vaniline (2-hydroxy-3-methoxybenzaldehyde) in 30 mL ethanol in a round-bottomed flask. The mixture was refluxed with continuous stirring using a hot-stage magnetic stirrer for nearly 2 hours. The off-white solid precipitate was filtered, washed with ethanol, dried, and finally recrystallized in hot ethanol. The yield obtained was 89%, and the measured melting point was 117°C.

Elemental analysis for $C_{19}H_{17}N_3O_4$: cal. (found), %C 65.01 (64.95), %H 4.84 (4.71), %N 11.97 (12.22), and %O 18.23 (17.86).

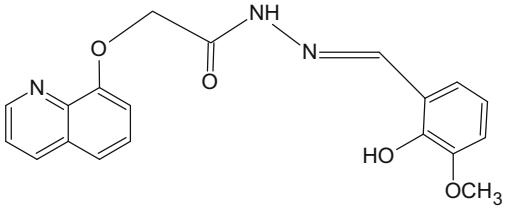

Figure 3: Structure of SL_2 ligand.

2.4.3 Synthesis of *N'*-[(*E*)-(2-hydroxynaphthalen-1-yl) methylidene]-2-[(quinolin-8-yl)oxy] acetohydrazide (SL_3)

SL_3 (Figure 4) was synthesized by condensation reaction using 0.01 mol of 2-(quinolin-8-yloxy)acetohydrazide and mixed with 0.01 mol 2-hydroxy-1-naphthaldehyde in 30 mL ethanol in a round-bottomed flask. The mixture was refluxed with continuous stirring using a hot-stage magnetic stirrer for nearly two and a half hours. The yellow solid precipitate was filtered, washed with ethanol, dried, and finally recrystallized in hot ethanol. The yield obtained was 94%, and the measured melting point was 180°C.

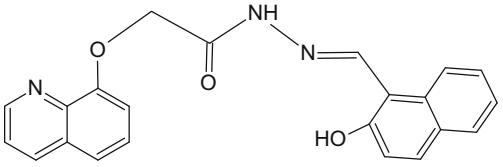

Figure 4: Structure of SL_3 ligand.

Elemental analysis for $C_{22}H_{17}N_3O_3$: cal. (found), %C 71.22 (71.63), %H 4.58 (4.54), %N 11.32 (11.59), and %O 12.94 (12.64).

2.4.4 Synthesis of *N'*-[(*E*)-(pyridin-3-yl)methylidene]-2-[(quinolin-8-yl)oxy]acetohydrazide (SL_4)

SL_4 (Figure 5) was synthesized by condensation reaction using 0.01 mol of 2-(quinolin-8-yloxy)acetohydrazide as a primary amine and mixed with 0.01 mol pyridine-3-carboxaldehyde as an aldehydic compound in 30 mL ethanol in a round-bottomed flask. The reaction mixture was refluxed with continuous stirring using a hot-stage magnetic stirrer for nearly 2 hours. The yellowish-white (beige) solid precipitate was filtered, washed with ethanol, dried, and finally recrystallized in hot ethanol.

The yield obtained was 78%, and the measured melting point was 105°C.

Elemental analysis for $C_{17}H_{14}N_4O_2$: cal. (found), %C 66.72 (66.33), %H 4.58 (4.85), %N 18.30 (18.71), and %O 10.46 (10.12).

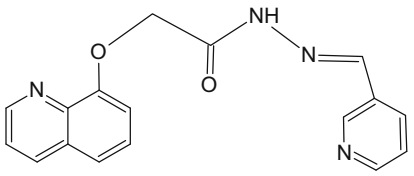

Figure 5: Structure of SL_4 ligand.

2.5 General procedure for preparation of metal complexes

The targeted Cu(II) and Zn(II) metal complexes were prepared by the general reported procedure [14]. A solution of metal salt dissolved in ethanol was mixed gradually with the ethanolic solutions of the Schiff bases (SL_1–SL_4) obtained as mentioned before in 1:2 (metal to ligand) molar ratio. The reaction mixture was refluxed with continuous stirring using a hot-stage magnetic stirrer for 4–6 h at nearly 90°C. The precipitated compounds obtained were separated by filtration, washed with hot ethanol, and finally with diethyl ether. The compounds were dried in open air; the yield, color, mass spectra, and elemental analysis are given later. The melting points for all metal complexes were above 300°C. The elemental analysis and physical characteristics of the prepared complexes are presented in Table 1.

2.6 Antimicrobial activity assessment – *in vitro* experimentation

The microbial susceptibility of the free organic ligands and their Cu(II) and Zn(II) metal complexes was assessed for their antimicrobial capacity against different pathogenic Gram-negative and Gram-positive bacterial strains and fungal strains. The two Gram-negative bacterial strains used in the experimentation were *P. aeruginosa* (*ATCC 27853*) and *E. coli* (*ATCC25922*), and the two Gram-positive bacterial strains used in the experimentation were *S. aureus* (*ATCC 25923*) and *E. faecalis* (*ATCC 29212*). For antifungal experimentation potentials, we used the common pathogenic yeast *C. albicans* (*ATCC10231*). The assessment experiments were performed *in vitro* at the Department of Clinical Microbiology, Blood Bank Centre, Al-Baha City, KSA. The method followed was agar disk-diffusion assessment method according to the Clinical and Laboratory Standards Institute (CLSI) [15]. Muller Hinton Agar was used as a growth medium for bacterial strains, while Sabouraud dextrose agar nutrient was used as a microbiological growth medium for fungal strains. Stock solutions of the examined compounds were prepared by dissolving 0.02 g of each compound in 5.0 mL DMSO solvent and used for experimental tests. DMSO solvent was used as the negative control. The common antibacterial amoxicillin and the antifungal fluconazole drugs were used as references for comparison. The zones of complete inhibition (in millimeters) after the incubation period were measured around every compound, which indicates the lethality of the tested compound on the microbial microorganisms in question.

2.7 *In silico* predictions

The prepared ligands and their metal complexes were subjected to *in silico* physicochemical investigation, and the number of rotatable bonds, lipophilicity, and topological polar surface area (TPSA) were calculated to understand the drug transport properties. *In silico* % age absorption was calculated using the reported formula [(%ABS = 109 − (0.345 × TPSA)] [16,17]. In addition, the *in silico* pharmacokinetic predictions were carried out to predict the absorption, distribution, metabolism, and elimination (ADME) for the targeted ligands, and their corresponding metal complexes were determined by Swiss ADME web interface (http//www.sib.swiss) [18]. The Lipinski, Ghose, Veber, Egan, and Muegge rules were applied to predict whether the targeted compounds are likely to be bioactive [19].

Ethical approval: The conducted research is not related to either human or animal use.

3 Results and discussion

3.1 Synthesis and characterization

The main purpose of this research work was to synthesize and characterize new Schiff base ligands incorporating quinoline moiety and to use them for preparing metal complexes with the transition metal ions Cu^{2+} and Zn^{2+}. To achieve this goal, the key primary

Table 1: Physical properties and elemental analysis of the synthesized Schiff base complexes

Metal complex	Mol. formula	Mol. wt.	Color	Yield (%)	Mass spectra (*m*/*z*)	Elemental analysis calculated (found) (%)				
						C	H	N	O	Metal
$[Cu(SL_1)_2]$	$CuC_{36}H_{28}N_6O_6$	703.5	Green	58.8	704.00	61.41 (61.82)	3.98 (4.15)	11.94 (11.63)	13.64 (13.73)	9.03 (8.86)
$[Zn(SL_1)_2]$	$ZnC_{36}H_{28}N_6O_6$	705.38	Off-white	72.99	705.08	61.24 (60.98)	3.96 (4.24)	11.90 (11.76)	13.60 (13.66)	9.26 (9.11)
$[Cu(SL_2)_2]$	$CuC_{38}H_{32}N_6O_8$	655.55	Turquoise green	68.13	763.92	69.55 (70.00)	4.88 (5.12)	12.81 (12.34)	19.52 (19.16)	9.69 (9.62)
$[Zn(SL_2)_2]$	$ZnC_{38}H_{32}N_6O_8$	765.38	Yellowish-white	79.89	765.33	69.36 (69.85)	4.86 (4.71)	12.77 (12.70)	19.47 (19.83)	9.94 (9.70)
$[Cu(SL_3)_2]$	$CuC_{44}H_{32}N_6O_6$	803.55	Light green	87.03	802.33	65.70 (66.02)	3.98 (4.12)	10.45 (10.22)	11.94 (11.50)	7.90 (8.14)
$[Zn(SL_3)_2]$	$ZnC_{44}H_{32}N_6O_6$	805.38	Yellowish-white	87.04	805.42	65.55 (65.68)	3.97 (4.16)	10.42 (10.36)	11.91 (12.35)	8.11 (8.26)
$[Cu(SL_4)_2]$	$CuC_{34}H_{26}N_8O_4$	673.55	Light brown	76.32	672.17	60.57 (60.95)	3.86 (4.12)	16.63 (16.27)	9.50 (9.17)	9.43 (9.40)
$[Zn(SL_4)_2]$	$ZnC_{34}H_{26}N_8O_4$	675.38	Whitish-yellow	58.5	675.08	60.41 (60.32)	3.84 (4.06)	16.58 (16.92)	9.47 (9.11)	9.68 (9.44)

amine compound 2-(quinolin-8-yloxy)acetohydrazide containing quinoline moiety was selected and synthesized in the laboratory following the reported procedure [11–13]. The structure of the key compound was confirmed before proceeding for the next step. Furthermore, the synthesized primary amine 2-(quinolin-8-yloxy)acetohydrazide was coupled with different aromatic aldehydes such as salicylaldehyde, *o*-vaniline, 2-hydroxy-1-naphthaldehyde, and pyridine-3-carboxaldehyde in (1:1) stoichiometric ratio to produce four different quinoline-hydrazone Schiff base ligands (SL_1–SL_4).

3.1.1 Characterization of the Schiff base ligands

The isolated Schiff bases were purified by recrystallization using hot ethanol and were in good yields (78–94%). They were mostly yellow colored and were soluble in hot ethanol, N,N-dimethylformamide (DMF), and dimethyl sulfoxide (DMSO). The isolated Schiff base ligands were characterized, and the proposed structures were confirmed before proceeding for the preparation of the targeted Cu(II) and Zn(II) metal complexes step. The elemental analysis results for C, H, N, and O found were in good agreement with the theoretically calculated percentage values for the proposed molecular formulae, in favor of the expected structures of the Schiff base ligands. The obtained mass spectra (*m*/*z*) for each of the prepared ligand compounds (SL_1–SL_4) were also in agreement with the molecular formulae of the prepared Schiff bases.

The IR spectrum of the organic Schiff base compounds exhibited characteristic peaks (Table 2), which were helpful in proving the proposed structures of the ligands. The sharp bands appeared at 1,500, 1,502, 1,504 and 1,505 in the spectrum of the ligands SL_1–SL_4, respectively, designed to the characteristic azomethine group (–CH═N–), which indicates the formation of the Schiff base ligands [20]. The presence of the aromatic (–OH) group in the spectrum of the ligands exhibited peaks at 3,500, 3,513, 3,570, and 3,606 cm^{-1}, respectively [21]. The intense bands observed in the range 1,225–1,255 in the IR spectrum of the ligands (SL_1–SL_3) are due to the phenolic C–O linkage [22]. The sharp transmission bands at 1,660, 1,665, 1,685, and 1,671 cm^{-1} in the spectra of SL_1, SL_2 SL_3, and SL_4, respectively, are due to the presence of the stretching carbonyl C═O group [9,12,23]. Weak transmission bands observed in the range 2,985–2,988 cm^{-1} may be assigned to the –N–H amide group [9,23]. The transmission bands observed at 1,115, 1,114, 1,110, and 1,112 cm^{-1} in the spectra of SL_1, SL_2 SL_3, and SL_4, respectively, can be assigned to the –N–N– linkage [24].

Table 2: Important characteristic IR bands (cm^{-1}) of the ligands and metal complexes

Compounds	$\nu_{C=N}$	ν_{OH}	ν_{C-O} (phenolic)	$\nu_{C=O}$ (carbonyl)	N_{N-H}	ν_{M-N}	ν_{M-O}	ν_{-N-N-}
SL_1	1,500	3,500	1,225	1,660	3,050	—	—	1,115
SL_2	1,502	3,513	1,255	1,655	3,045	—	—	1,114
SL_3	1,504	3,570	1,242	1,685	2,995	—	—	1,110
SL_4	1,505	3,606	—	1,671	2,988	—	—	1,112
$[Cu(SL_1)_2]$	1,534	—	1,252	1,653	3,012	480	586	1,112
$[Zn(SL_1)_2]$	1,550	—	1,261	1,659	3,062	484	571	1,114
$[Cu(SL_2)_2]$	1,541	—	1,212	1,684	2,988w	479	583	1,110
$[Zn(SL_2)_2]$	1,543	—	1,223	1,653	3,015	456	577	1,115
$[Cu(SL_3)_2]$	1,553	—	1,211	1,662	3,021w	451	532	1,114
$[Zn(SL_3)_2]$	1,557	—	1,218	1,684	3,050	462	569	1,113
$[Cu(SL_4)_2]$	1,545	—	—	1,670	3,010	451	568	1,112
$[Zn(SL_4)_2]$	1,540	—	—	1,663	3,024w	488	542	1,127

w = weak band.

The observed UV-visible absorption spectra for the free organic Schiff base ligands (SL_1–SL_4) show two main bands. The first observed at lower wavelength bands at 295, 284, 262, and 301 nm in the spectrum of the ligands SL_1, SL_2, SL_3, and SL_4, respectively, that can be assigned to $\pi \rightarrow \pi^*$ transitions within the benzene and quinoline rings [25,26]. The second bands were observed at 324, 326, 322, 317 nm in the spectrum of the ligands SL_1, SL_2, SL_3, and SL_4, respectively, which may involve $\pi \rightarrow \pi^*$ and $n \rightarrow \pi^*$ transitions of the (–C═N–) group [26].

In the ^{1}H NMR Spectra of all the Schiff base ligands (SL_1–SL_4), the imine protons were observed at 8.58–8.98 ppm as a singlet. Moreover, the peaks at 11.05–12.23 ppm, which are singlets, can be attributed to aromatic –OH protons in the ligand SL_1, SL_2, and SL_3 [27]. This shift in the position of the singlet may be due to the possibility effect of the formation of intramolecular hydrogen bonding interaction. The singlets appeared in the range of 12.18–12.52 ppm in the ^{1}H NMR spectrum of all Schiff base ligands are due to the –NH– linkage [28]. The peaks due to the aromatic hydrogens appeared in the range of 7.00–8.98 ppm [29].

In ^{13}C NMR spectra of the ligands SL_1, SL_2, SL_3, and SL_4, the peaks appeared at 148.75, 148.48, 147.62, and 145.69 ppm, respectively, are assigned to the carbon atom of the azomethine group [27]. The singlet peaks observed in the range of 164.81–169.57 ppm is due to the carbon atom of the C═O group [30]. Moreover, the peaks observed in the region 109.00–154.49 ppm are because of the carbon atoms of the aromatic ring [9].

3.1.2 Synthesis and characterization of metal complexes

Copper(II) and Zinc(II) from the first transition elements series of the d-block elements were chosen for the synthesis of the designed metal complexes in this research project. These metals are familiar, important metals and form interesting coordination compounds.

The targeted coordination metal complexes were prepared successfully by reacting to the metal salts of the selected metals with the prepared Schiff base ligands (SL_1–SL_4) in (1:2) stoichiometric ratio according to the described template method. The separated metal complexes were stable solids at room temperature and nonhygroscopic. They were solids insoluble in common organic solvents but soluble in DMF and DMSO. They were purified by recrystallization from hot DMF and DMSO solvents. All prepared metal complexes had high melting points (above 300°C).

The elemental analysis measurements suggested 1:2 metal to ligand stoichiometric ratio forming tetra-coordinate monomeric Cu(II) and Zn(II) metal complexes. The measured percentages of the carbon, hydrogen, nitrogen, oxygen, and metal ion are in agreement with the calculated ones according to the suggested structure of the complexes as shown in Figure 6(a–d). The Schiff base quinoline acetohydrazone ligands containing NO coordination sites behave as monobasic bidentate ligands. The general formula for the prepared complexes suggested to be $[M(SL_{1-4})_2]$ for all metal complexes

According to the above-proposed structures, the prepared Cu(II) and Zn(II) complexes are suggested to be mononuclear complexes. The ligands SL_1–SL_3 bind to metal ions through the nitrogen atom of the azomethine (–CH═N–) group and the oxygen atom of the phenolic (–OH) group forming square planar geometry. Moreover, the bidentate Schiff base ligands SL_1, SL_2, and SL_3 forms six-membered chelate rings at the Cu(II) and Zn(II) acceptor centers. The ligand SL_4 binds to metal ions through the N atom of –C═N– group and the O atom of

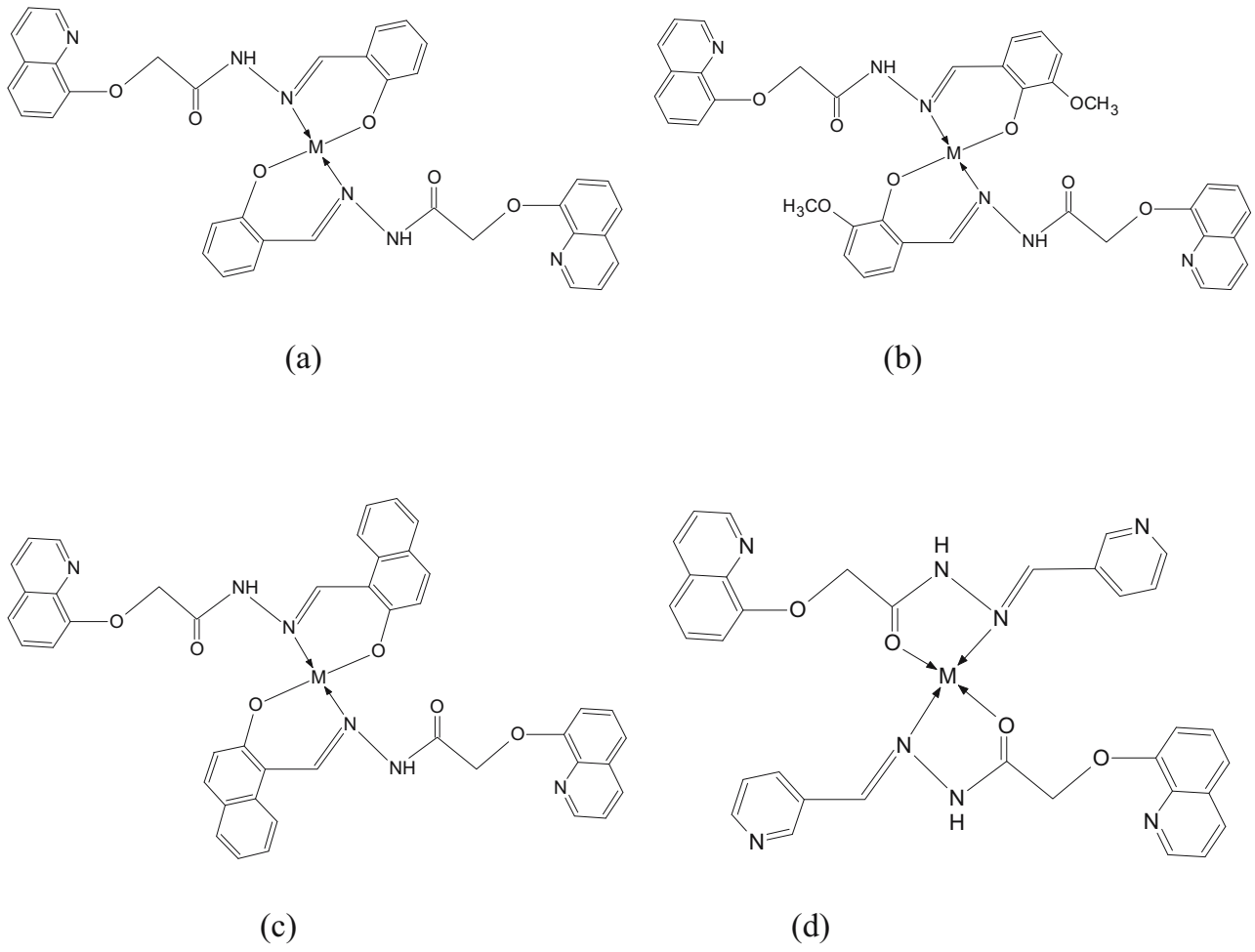

Figure 6: Structure of the synthesized complexes with (a) SL_1, (b) SL_2, (c) SL_3, and (d) SL_4 where M = Cu(II) or Ni(II).

the carbonyl group forming square planar geometry. The bidentate SL_4 ligand forms a five-membered ring at the metal acceptor center.

To prove the proposed structures for the prepared metal complexes, we performed different analytical techniques. Mass spectrometry analysis was carried out to help in quantifying and structure elucidation of the obtained complexes and confirm the molecular weights. The measured (m/z) peaks indicated that the observed molecular peaks for all prepared metal complexes are equivalent to the theoretically calculated formula weights according to the proposed structures. These observations support and prove the suggested structures for the prepared metal complexes shown in Figure 6(a–d).

The comparison between the IR spectral data of the free organic ligands (SL_1–SL_4) and that of the corresponding Cu(II) and Zn(II) metal complexes demonstrate that the ligands were binding to the metal ions. The coordination of the ligands through the nitrogen atom of the azomethine group was indicated through the shift (blue shift) of the νC═N band in the IR spectrum of the complexes when compared with the free organic ligands. This also was supported by the appearance of the new weak band in the spectrum of the metal complexes at the range of 437–488 cm^{-1} attributed to the formation of M–N bonds [1]. The formation of M–N bond leads to the weakening of the C═N band due to the donation of electrons from the nitrogen atom to the vacant d-orbitals in the metal atoms, which causes the shift of the azomethine band in the metal complexes [16].

The bands (3,500, 3,513, 3,570, and 3,606 cm^{-1}) shown in the IR spectrum of the free Schiff bases (SL_1–SL_3) due to the phenolic (νOH) group were disappeared in the IR spectrum of the corresponding Cu(II) and Zn(II) complexes. This is a sign of the binding of the oxygen atom of the phenolic group to the metal atoms [22,31]. Moreover, the intense bands observed in the IR spectrum of the ligands (SL_1–SL_3) due to the

phenolic C–O linkage were shifted and appeared in the range of 1,211–1,265 cm^{-1} is another proof for the involvement of the OH group in bonding with the metal ions [22]. In addition, a weak band was observed in the IR spectrum of these complexes at the range of 542–595 cm^{-1} which is assigned to the νM–O mode, evidence for the formation of M–O bonds [32,33].

It was also observed that the band 1,671 cm^{-1} due to the νC=O of the carbonyl group in the IR spectrum of SL_4 ligand was shifted slightly in the spectrum of the corresponding metal complexes, which indicate the binding of the oxygen atom to the metal ions [33].

The most important bands observed in the IR spectrum of the metal complexes are shown in Table 2.

The UV-visible and magnetic moment susceptibility (μ_{eff}) data are helpful tools to deduce the nature of the ligand field around the metal ion and the geometry of the obtained metal complexes. The observed UV-visible transmission bands for the prepared Cu(II) and Zn(II) complexes are shown in Table 3. The UV-visible spectra indicate that there is a relative shift to lower wavelengths (bathochromic shift) of the transmission bands due to π–π^* and n–π^* transitions that observed in the spectrum of the free prepared Schiff base ligand. This observation may be because of the coordination of the ligands to the metal core, which causes a change in the distribution of electrons between the ligands and the metal ions [25,26,34,35].

The discussion for each metal complexes is discussed in the following sections.

3.1.3 Cu(II) metal complexes

The observed UV-visible spectra of the synthesized mononuclear copper(II) complexes showed transmission bands in the range λ_{max} = 648–675 nm, which may be accountable for the $2B_{1g} \rightarrow 2A_{1g}$ transitions that are consistent with square-planar geometry around the Cu(II) centers [36,37]. Moreover, the magnetic moment values (Table 3) were between 1.906 and 2.261 BM which lies within the permissible values reported for one unpaired electron, and it is an evident that supports the square-planar geometry of Cu(II) complexes [37]. This geometry is achieved through the coordination of two bidentate ligands (SL_1–SL_4) to the metal center in trans-geometry with respect to each other as shown in Figure 6(a–d).

Table 3: UV-visible transmission bands and μ_{eff} values for the metal complexes

Compound	Transmission bands (λ_{max} in nm)	Magnetic moment μ_{eff} (B.M.)
$[Cu(SL_1)_2]$	305, 385, 661	1.961
$[Zn(SL_1)_2]$	277, 418, 685	Diamagnetic
$[Cu(SL_2)_2]$	313, 390, 675	2.261
$[Zn(SL_2)_2]$	305, 415, 610	Diamagnetic
$[Cu(SL_3)_2]$	321, 377, 650	1.924
$[Zn(SL_3)_2]$	273, 428, 622	Diamagnetic
$[Cu(SL_4)_2]$	345, 374, 648	1.906
$[Zn(SL_4)_2]$	269, 433, 612	Diamagnetic

3.1.4 Zn(II) complexes

The transmission bands observed in the range 269–277 nm in the UV-visible spectrum of Zn(II) complexes can be assigned to the $\pi \rightarrow \pi^*$ transitions. The weak bands in the range of 305–318 nm were assigned to $n \rightarrow \pi^*$ transitions. Moreover, the bands observed in the range 423–438 nm may be attributed to the ligand-to-metal charge transfer transitions [27,38]. The lowest energy bands at the range 610–685 nm were due to the $d \rightarrow d$ transition of Zn^{2+}. These observations are consistent with square-planar geometry. The observed magnetic moment (Table 3) for all Zn(II) complexes were diamagnetic, which is in support of the square-planar geometry [27,38].

The four-coordinated mononuclear complexes of Zn (II) are achieved through the coordination of the bidentate (SL_1–SL_4) ligands to the metal center in trans-geometry with respect to each other as shown in Figure 6(a–d). The coordination is through two N atoms and two oxygen atoms from two same Schiff base ligands in a square-planar geometry.

The ^1H NMR analysis was further performed to achieve concrete evidence of the binding of the Cu^{2+} and Zn^{2+} to the ligands. Upon complexation, the peaks due to the proton of the imine group in the Schiff base ligands were showed field up shift slightly by Δ_δ = 0.40–0.80 ppm. The singlet peaks due to the phenolic proton in the ^1H NMR spectra of SL_1, SL_2, and SL_3 were disappeared indicating the deprotonation of this group. These observations proved that the N atom of the azomethine (>CH=N–) group and the O atom of the phenolic (–OH) group participate in coordination and formation of the metal complexes [27]. The peaks observed for the –NH– proton did not show any shift and remained at the same position in the spectra of the metal complexes, which were an indication of no-participation of this group in bonding to the metal ions.

Thermal analysis studies of some prepared metal complexes were investigated at the heating rate of 10

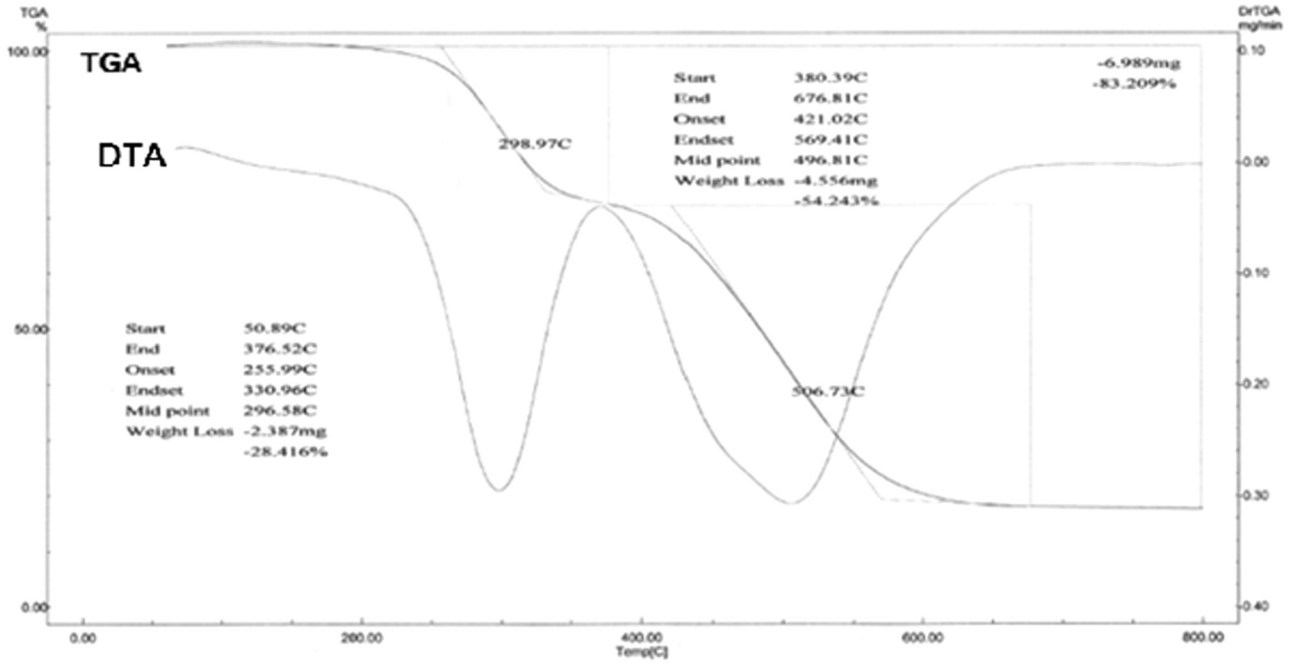

Figure 7: TGA–DTA curves of $[Zn(SL_1)_2]$.

(°C/min) under the nitrogen atmosphere from room temperature to 800°C. These thermogravimetric studies are helpful tools and good supports in the characterization of the prepared metal complexes.

The results of representative TG/DTA plots of the analyzed metal complexes are shown in Figure 7 and 8. The results show good harmony with the proposed chemical structures suggested from the analytical data as discussed earlier. It is obvious from the decomposition pattern that the studied metal complexes were decomposed in three successive stages. The TGA curves of anhydrous complexes do not display any mass losses up to 260°C, which indicate the thermal stability of the metal complexes and confirm the absence of water molecules in the complex structures. In Figure 7, the first step for the complex $[Zn(SL_1)_2]$ (molecular weight = 706.3) started decomposition between 256 and 331°C and weight loss observed was 28.416% which is corresponding to two molecules of the salicylaldehyde part from

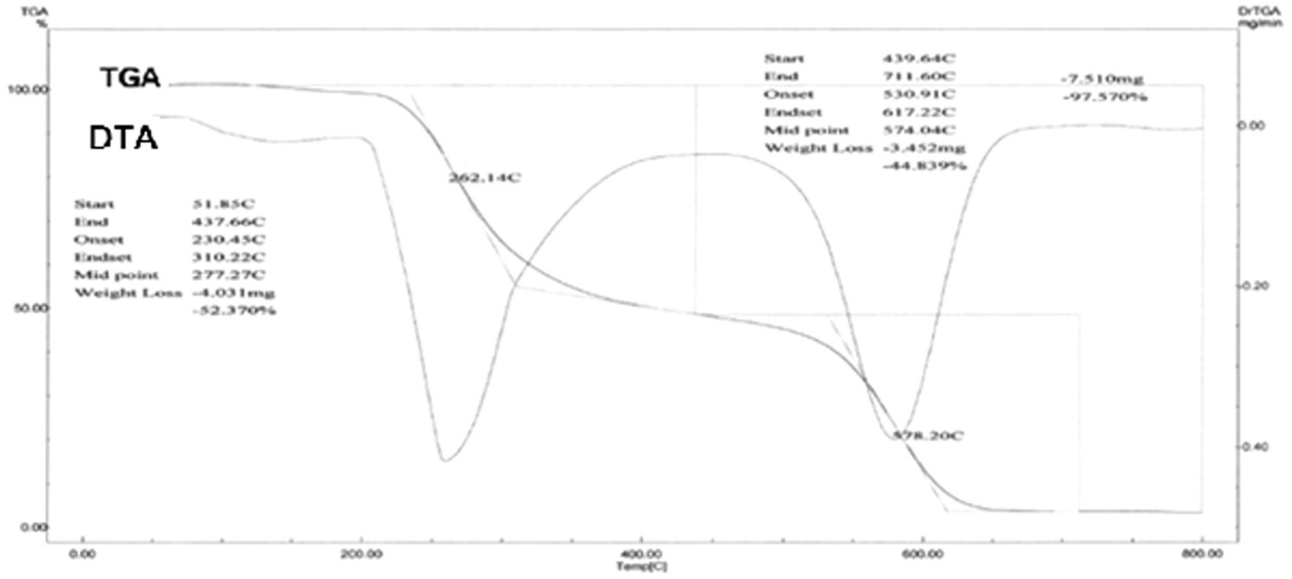

Figure 8: TGA–DTA curves of $[Zn(SL_3)_2]$.

the ligand (i.e., $C_{14}H_{12}$) (calculated weight percentage 30.02%) may be due to breaking the azomethine linkage during heating. The second step of decomposition was between 421.02 and 569.41°C with an observed weight loss of 54.243%, which can correspond to the ligand and aromatic ring (C_6H_4) (calculated weight percentage 54.44%). The third step on further heating above 600°C, metal complexes decompose to stable zinc oxide. In Figure 8, the first step for the decomposition of $[Zn(SL_3)_2]$ (molecular weight = 806.15) started decomposition between 230 and 310°C and weight loss observed was 52.37% which is corresponding to two molecules of the amine part (i.e., $C_{22}H_{18}O_4N_6$) from the organic ligand (calculated weight percentage 53.35%). In the second step, the observed weight loss was 44.83% which corresponds to the organic ligand ($C_{22}H_{17}N_3O_3$) (calculated weight percentage = 46.02%). Final step above 630°C decompose the complex to the stable zinc oxide. In the DTA curve of the metal complexes, the heat flow in the 90–600°C temperature range was shown as endothermic peaks.

Table 4: The measured molar conductivity for the metal complexes

Metal complex	Molar conductance ($\Omega^{-1}\,cm^2\,mol^{-1}$)
$[Cu(SL_1)_2]$	7.22
$[Zn(SL_1)_2]$	7.26
$[Cu(SL_2)_2]$	6.32
$[Zn(SL_2)_2]$	27.9
$[Cu(SL_3)_2]$	2.16
$[Zn(SL_3)_2]$	35.4
$[Cu(SL_4)_2]$	12.6
$[Zn(SL_4)_2]$	11.8

3.2 Molar conductance of the prepared metal complexes

To examine the electrolytic or nonelectrolyte nature of the prepared metal complexes, we measured the molar conductance (Λm) of freshly prepared 1.0×10^{-3} M solutions of the synthesized metal coordination compounds in DMSO at room temperature (24°C). The measured values are presented in Table 4. The molar conductance values obtained were in the range (2.16–35.4 $\Omega^{-1}\,cm^2\,mol^{-1}$) which are considered very low. It is evident from these results that the prepared Cu(II) and Zn(II) complexes are nonionic in nature (non-electrolytes). Moreover, it is confirmed that the ligands are involved in the coordination sphere [38,39].

3.3 *In vitro* anti-microbial potentials

The free prepared organic ligands (SL_1–SL_4) and their corresponding Cu(II), and Zn(II) metal complexes were assayed *in vitro* for their potential antibacterial and antifungal activities utilizing the agar disc-diffusion method. The zones of complete inhibition (in millimeters) were measured, and the observations are presented in Table 5 as arithmetic mean values.

Table 5: Antimicrobial observations for the ligands and their Cu(II) and Zn(II) complexes

Compound	Zone of inhibition (mm)				
	Gram-positive bacteria		Gram-negative bacteria		Fungus
	S. aureus	*E. faecalis*	*E. coli*	*P. aeruginosa*	*C. albicans*
SL_1	19	21	7	0	0
SL_2	22	23	0	0	0
SL_3	24	08	0	0	0
SL_4	20	20	0	0	0
$[Cu(SL_1)_2]$	31	32	12	0	0
$[Zn(SL_1)_2]$	18	18	0	0	0
$[Cu(SL_2)_2]$	24	0	0	0	3
$[Zn(SL_2)_2]$	25	28	0	0	0
$[Cu(SL_3)_2]$	25	15	6	0	0
$[Zn(SL_3)_2]$	29	30	13	0	0
$[Cu(SL_4)_2]$	26	11	0	0	0
$[Zn(SL_4)_2]$	9	0	0	0	0
Amoxicillin	40	38	23	—	17
Fluconazole	36	35	35	37	42

The ligands (SL_1–SL_4) exhibited moderate antibacterial activity against the Gram-positive bacterial types with zones of inhibitions in the range of 8–25 mm. They showed no activity against the Gram-negative bacterial types and the fungal strain too. SL_3 ligand compound showed the highest activity when compared with other ligands with a zone of inhibition of 24 mm against *S. aureus*. Compared to the amoxicillin and fluconazole as standards, the activity of the ligands was much lower.

The corresponding metal complexes, in general, showed some enhancement antibacterial activity against both Gram-positive *S. aureus* and *E. faecalis* bacterial strains with zones of inhibitions in the range of 18–32 mm. While similar to the parent ligands, the complexes showed no activity against the Gram-negative bacterial stains and the fungal strain. Few metal complexes showed weak activity against the Gram-negative bacteria *E. coli* with zones of inhibition less than 15 mm. On comparing between the metal complexes, it was observed that $[Cu(SL_1)_2]$ was the most toxic compound against the Gram-positive bacteria. $[Cu(SL_1)_2]$ exhibited activity with zones of inhibition of 31 and 32 mm against *S. aureus* and *E. faecalis*, respectively. On comparing the activities of the metal complexes with the standard drugs, the metal complexes exhibited less antibacterial and antifungal activity.

Based on the Tweedy's chelation theory and Overtone's permeability principles, the antibacterial enhancement activity of the metal complexes can be interpreted [40]. According to the chelation theory, the coordination of organic ligands with metals reduces the polarity of the metal due to overlap of the orbitals of the ligand with the metal orbitals and the generation of delocalized π-electrons over the entire coordination sphere. This enhances the liposolubity and influences the cell membrane permeability of the metal complexes into the microbial cell [1,40]. This facilitation in the lipophilicity and penetration of the metal complexes inside the microbial cell give rise to adverse effects in the cell environment and enzymes of the cell and further affects the proliferation of the microorganism [20,41]. Moreover, the possibility of the formation of hydrogen bonds through the >CH=N– group with cell components can cause and interfere with normal cell processes [31].

The higher activity of the Cu(II) complexes compared to the Zn(II) complexes may be interpreted on the stability of these complexes [42].

Figures 9 and 10 show some photographs of the antibacterial and antifungal tests.

3.4 *In silico* prediction

New drug discovery and development demand considerable facilities, materials, and time. For this reason, theoretical investigations have a major role in reducing these factors and predicting the possibility of prospective drug applications. It is not sufficient for a chemical to show *in vitro* excellent biological activities, but in addition, it is required to satisfy the pharmacokinetic parameters ADME. These parameters can be validated by the *in silico* investigations through computing the physicochemical criteria.

3.4.1 Physicochemical properties

The pharmacological or therapeutic effect is related to the influence of various physicochemical properties of

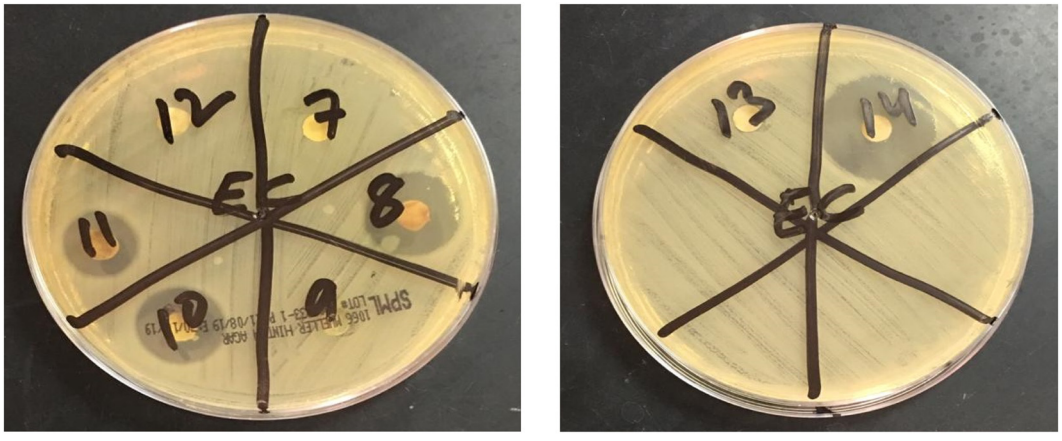

(a) (b)

Figure 9: Photographs of some antibacterial tests against *S. aureus* bacterial strains. (a) Shows some of the active compounds 8 = SL_3, 10 = $[Zn(SL_3)_2]$ and 11 = $[Cu(SL_3)_2]$; (b) shows the activity of compound 14 = $[Cu(SL_1)_2]$.

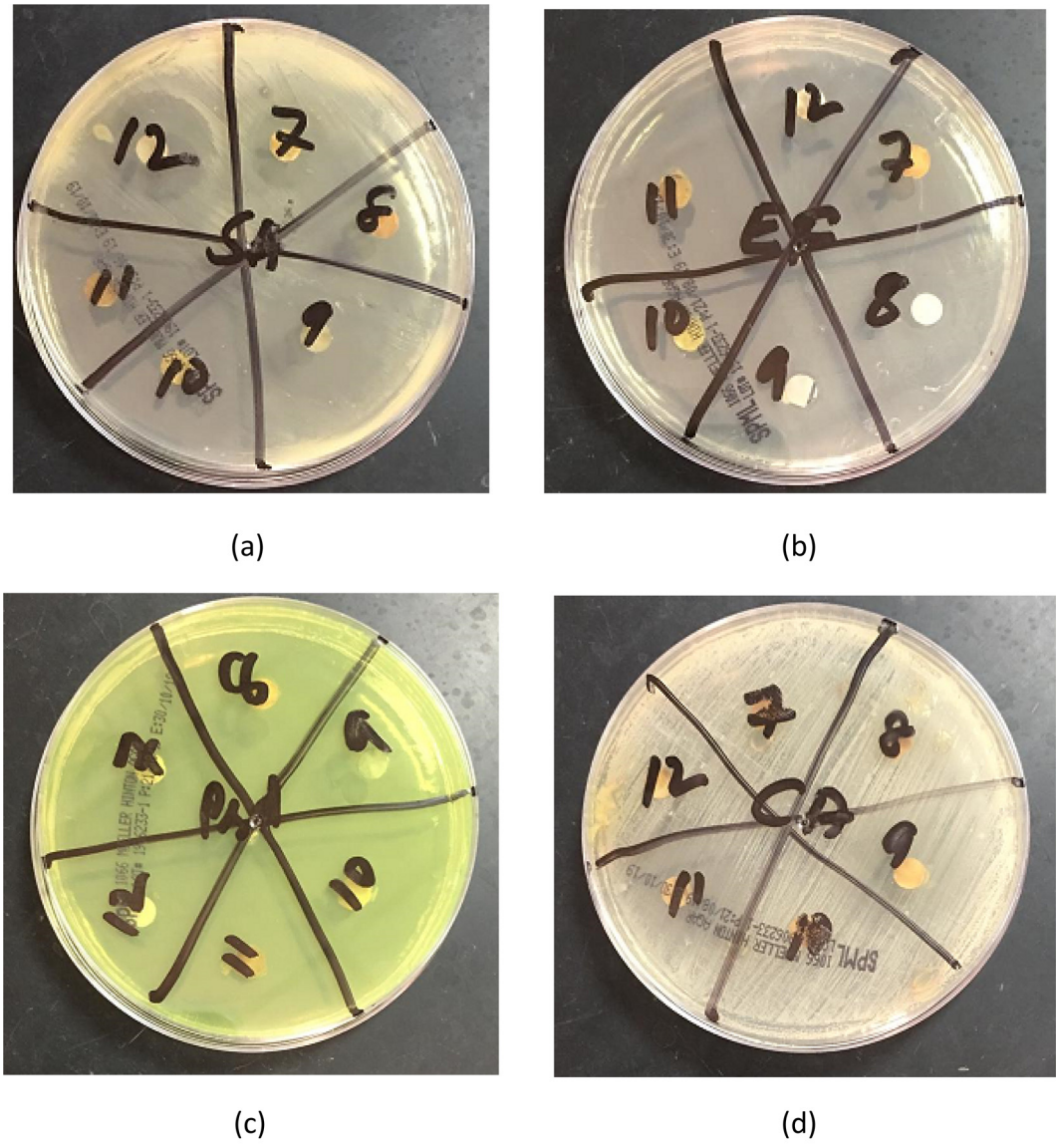

Figure 10: Representative photographs for antibacterial and antifungal tests for each strain used: (a) *E. faecalis*, (b) *E. coli*, (c) *P. aeruginosa*, (d) *C. albicans*.

the chemical on the biomolecules that it interacts with. Different physicochemical parameters of a drug candidate play a crucial role in their pharmacokinetic behavior [43]. In view of this, their calculation and measurement help in prioritizing compounds for screening as an efficient drug candidate and enable preliminary decisions in drug discovery [44]. The prepared ligands and their metal complexes were subjected to *in silico* physicochemical studies such as number of rotatable bonds, hydrogen bond acceptor, hydrogen bond donor, molecular reactivity, water-solubility, lipophilicity, and topological polar surface area (TPSA), which were calculated for understanding the drug transport properties. All results obtained are presented in Table 6. The results of *in silico* absorption percentage calculations indicated that the percentage of absorption was in the range of 76.90–82.61% among ligands, where the ligand SL_4 was the highest with an absorption percentage of 82.61%. The *in silico* absorption percentage (42.84–56.23) among complexes observations showed that the complexes $[Cu(SL_4)_2]$ and $[Zn(SL_4)_2]$ showed the highest absorption percentage with the value of 56.23% for both complexes. On comparing the ligands and their corresponding metal complexes, it is clear that the ligands showed a much higher absorption percentage. Moreover, the obtained TPSA values for the ligands were below 140 $Å^2$ (the accepted limit of polar surface area), indicating that ligands had considerable

Table 6: Physicochemical properties of the ligands and their complexes

Compound no.	Fraction Csp^3 [a]	No. of rotatable bonds	HBA[b]	HBD[c]	MilogP[d]	Molar refractivity	ESOL log *S*[e]	TPSA[f]	*In silico* % absorption
SL_1	0.06	6	5	2	1.96	91.05	−3.68	83.81	80.08
SL_2	0.11	7	6	2	2.7	97.54	−3.74	93.04	76.90
SL_3	0.05	6	5	2	2.61	108.55	−4.81	83.81	80.08
SL_4	0.06	6	5	1	1.74	86.82	−3.16	76.47	82.61
$[Cu(SL_1)_2]$	0.06	16	10	2	0	179.3	−7.53	173.28	49.20
$[Zn(SL_1)_2]$	0.06	16	10	2	0	179.3	−7.54	173.28	49.20
$[Cu(SL_2)_2]$	0.11	18	12	2	0	192.29	−7.7	191.74	42.84
$[Zn(SL_2)_2]$	0.11	18	12	2	0	192.29	−7.71	191.74	42.84
$[Cu(SL_3)_2]$	0.05	16	10	2	0	214.31	−9.76	173.28	49.20
$[Zn(SL_3)_2]$	0.05	16	10	2	0	214.31	−9.78	173.28	49.20
$[Cu(SL_4)_2]$	0.06	12	10	2	36.16	173.64	−6.35	152.94	56.23
$[Zn(SL_4)_2]$	0.06	12	10	2	−45.4	173.64	−6.36	152.94	56.23

[a]The ratio of sp^3 hybridized carbons over the total carbon count of the molecule. [b]Number of hydrogen bond acceptor. [c]Number of hydrogen bond donor. [d]Lipophilicity. [e]Water solubility. [f]Topological polar surface area ($^0A^2$). ESOL = estimated solubility.

permeability into the cellular plasma membrane [45]. While the TPSA values for the examined metal complexes were very high (>140 Å^2) marking low permeability into the cellular plasma membrane. The log *S* (that is the coefficient of solubility determined by the estimated solubility (ESOL) method computed on Swiss ADME) for many known drugs available in the market showed values more than −4.00 [45]. In our investigation, the obtained values of log *S* (Table 6) for the ligands SL_1, SL_2, and SL_4 were little more than −4.00, indicating that these compounds are considered moderate soluble. While SL_2 was having a value of (−4.81) which is less and hence this compound considered insoluble. In the case of the metal complexes, the log *S* values are much less than (−4.00), and hence, the metal complexes are considered highly insoluble.

3.4.2 *In silico* pharmacokinetic/ADME and drug-likeness properties

Pharmacokinetics is used to investigate the time course of chemical absorption, distribution, metabolism, and excretion (ADME) and determines the fate of the chemical administered to the living organisms. In this paper, we have performed *in silico* pharmacokinetic predictions for the prepared four Schiff base ligands (SL_1–SL_4) and the prepared corresponding Cu(II) and Zn(II) metal complexes and the obtained results are presented in Table 7. The gastrointestinal (GI) absorption score measures the extent of absorption of a chemical from the intestine, the results pointed out that all the ligands have high GI absorption and hence had excellent absorption possibility from the intestine after oral administration, while the complexes showed low GI absorption and hence had low absorption possibility from the intestine. It was very interesting that all the ligands and complexes were unable to penetrate through the blood–brain barrier (BBB) except the ligand SL_4. Besides this drug-likeness is the other parameter, which gives the probability of the molecules for the drug candidate. In the light of the drug-likeness definition, the chemical has a logarithm of the partition (log *P*) (i.e., octanol/water partition coefficient used to predict the solubility of a probable oral drug) between −0.4 and 5.6 values [46]. The skin permeability coefficient (K_p) is a criterion that considers the octanol/water partition coefficient to be a direct effect on the transdermal movement of chemical molecules and used to quantitatively describe the potential of dermal absorption for the synthesized compounds. In our study, log K_p values for all examined ligands and complexes were in the range of −7.50 to −5.04, which are below −0.4 indicating low lipophilicity and cannot penetrate through the lipid bilayers of the cells and suggesting that the synthesized compounds have bad drug-likeness. In addition, to discriminate between the drug-like and non-drug-like chemical substances, the Lipinski (rule-of-five) that describes the relationship between pharmacokinetic and physicochemical parameters, Ghose, Veber, Egan, and Muegge rules were applied to predict whether the target compounds are likely to be bioactive and assess qualitatively the chance of these compounds to become oral drug candidates [19]. The number of violations to these rules is listed in Table 8. All the ligands fulfilled Lipinski rule and other rules and showed zero violation

Table 7: Pharmacokinetic/ADME (absorption, distribution, metabolism, and excretion) properties of the ligands and complex compounds

Compound no.	Pharmacokinetic/ADME properties								
	GI Abs[a]	BBB Permeant[b]	P-gp Substrate[c]	CYP1A2 Inhibitor[d]	CYP2C19 Inhibitor[e]	CYP2C9 Inhibitor[f]	CYP2D6 Inhibitor[g]	CYP3A4 Inhibitor[h]	log K_p[i]
SL_1	High	No	No	Yes	No	Yes	Yes	No	−6.29
SL_2	High	No	No	Yes	No	Yes	Yes	Yes	−6.49
SL_3	High	No	No	Yes	Yes	Yes	Yes	Yes	−5.7
SL_4	High	Yes	No	Yes	Yes	Yes	Yes	No	−6.7
$[Cu(SL_1)_2]$	Low	No	No	No	No	Yes	No	Yes	−6.2
$[Zn(SL_1)_2]$	Low	No	No	No	No	Yes	No	Yes	−6.21
$[Cu(SL_2)_2]$	Low	No	No	No	No	Yes	No	Yes	−6.61
$[Zn(SL_2)_2]$	Low	No	No	No	No	Yes	No	Yes	−6.62
$[Cu(SL_3)_2]$	Low	No	Yes	No	No	No	No	Yes	−5.04
$[Zn(SL_3)_2]$	Low	No	Yes	No	No	No	No	Yes	−5.05
$[Cu(SL_4)_2]$	Low	No	Yes	No	No	No	No	No	−7.49
$[Zn(SL_4)_2]$	Low	No	Yes	No	No	No	No	No	−7.5

[a]Gastro intestinal absorption. [b]Blood–brain barrier permeant. [c]P-glycoprotein substrate. [d]CYP1A2: cytochrome P450 family1 subfamily A member 2(PDBHI4). [e]CYP2C19: cytochrome P450 family2 subfamily C member 19(PDB4GQS). [f]CYP2C9: cytochrome P450 family2 subfamily C member 9 (PDB1OG2). [g]CYP2D6: cytochrome P450 family 2 subfamily D member 6 (PDB5TFT). [h]CYP3A4: cytochrome P450 family 3 subfamily A member 4 (PDB4K9T). [i]Skin permeation in cm/s.

against all the rules, while all the complexes showed two violations against the Lipinski rule and different violations against the other rules. All the ligands in the screening processes showed good bioavailability with a score of 0.55, which is an indication that all organic ligands reach the circulation system, whereas the complexes showed moderate to poor bioavailability with scores in the range 0.11–0.17 and hence cannot reach the circulation system easily.

The prediction of the interaction of the tested compounds with cytochromes CYP450 major isoforms (CYP1A2, CYP2C19, CYP2C9, CYP2D6, and CYP3A4) was performed in order to check which compound will cause significant pharmacokinetic interactions that lead to toxic effect through inhibition of these isoenzymes. The CYP450 inhibition prediction results (Table 7) indicated that all synthesized ligands have probable inhibition to the CYP1A2, CYP2C9 and CYP2D6 isoforms. The ligand SL_3 showed inhibition possibility for all CYP450 isoforms. The majority of metal complexes showed inhibition possibility to the CYP3A4 isoform and no inhibition to the other CYP450 isoforms. The complexes with SL_4 ligand $[Cu(SL_4)_2]$ and $[Zn(SL_4)_2]$ showed no inhibition to all isoforms. Moreover, the probability of the compounds to be the substrate of P-glycoprotein (P-gp) was suggesting that ligands and the majority of complexes

Table 8: Drug likeness predictions of the target compounds

Compounds no.	Lipinski violations	Ghose violation	Veber violation	Egan violation	Muegge violation	Bioavailability score
SL_1	0	0	0	0	0	0.55
SL_2	0	0	0	0	0	0.55
SL_3	0	0	0	0	0	0.55
SL_4	0	0	0	0	0	0.55
$[Cu(SL_1)_2]$	2	3	2	1	4	0.11
$[Zn(SL_1)_2]$	2	3	2	1	4	0.11
$[Cu(SL_2)_2]$	2	3	2	1	5	0.11
$[Zn(SL_2)_2]$	2	3	2	1	5	0.11
$[Cu(SL_3)_2]$	2	4	2	2	5	0.11
$[Zn(SL_3)_2]$	2	4	2	2	5	0.11
$[Cu(SL_4)_2]$	2	3	2	1	2	0.17
$[Zn(SL_4)_2]$	2	3	2	1	2	0.17

have a probability to be nonsubstrate of P-gp. The complexes obtained from SL_3 and SL_4 showed a probability to be the substrate of P-gp. These results suggesting the more favor of non-drug-likeness of the tested compounds.

4 Conclusion

We have successfully prepared four new Schiff base ligands (SL_1–SL_4) with a quinoline hydrazine scaffold. The prepared Schiff base ligands were characterized, and their structures were proved before proceeding for the next step. A series of Cu(II) and Zn(II) complexes were synthesized using these ligands. The chemical and spectroscopic analyses results revealed that the ligands behaved as bidentate ligands and coordinated to the Cu(II) and Zn(II) metal ions through the N atom of the azomethine group and the O atom of the phenolic group or the ketonic O atom in case of SL_4 ligand and forming square-planar geometry. All the complexes were mononuclear and the general formula for complexes obtained from the ligands was of the type $[M(SL_{1-4})_2]$.

For proving the proposed structures of synthesized ligands and their corresponding metal complexes, we performed elemental analysis and various spectroscopic measurements, which showed similarities with the theoretically expected results indicating the formation of the compounds and proving their structures. Moreover, for metal complexes thermal analysis, magnetic moment and molar conductance measurements were investigated, and the results were in support of the estimated structures. Molar conductance measurement experimentation showed that the metal complexes were nonelectrolytic in nature. All synthesized ligands and complexes were screened for *in vitro* for testing antibacterial and antifungal activities. The organic ligands (SL_1–SL_4) exhibited moderate antibacterial activity against the Gram-positive bacterial types with zones of inhibitions in the range of 8–25 mm, which is much less than the standard reference drug. They were inactive against the Gram-negative bacteria and fungus strains and showed no zones of inhibition. The metal complexes showed some enhancement in the activity against the Gram-positive bacterial strains and were inactive against the Gram-negative bacteria and the fungus strains similar to the parent ligands. $[Cu(SL_1)_2]$ complexes were the most toxic compounds against both Gram-positive *S. aureus* and *E. faecalis* bacteria, but still less than the reference drugs.

In silico physicochemical investigation revealed that among the ligands, the ligand SL_4 showed highest *in silico* absorption with 82.61% and $[Cu(SL_4)_2]$ and $[Zn(SL_4)_2]$ complexes showed highest *in silico* absorption percentage of 56.23% among the complexes. The *in silico* pharmacokinetics predictions showed that the ligands have high GI absorption and the complexes showed low GI absorption. The ligands showed a good bioavailability score of 0.55 where the complexes showed moderate to poor bioavailability.

Finally, we recommend further investigations on the Schiff base ligands containing quinoline moiety and preparation of metal complexes using other metal ions and examining their biological activities. Moreover, other investigations are going on for their applications as catalysts, corrosion inhibitors, using these Schiff base ligands as chemosensors for the detection of heavy metal ions in different sources.

Acknowledgment: The authors are very grateful to the Head of the Chemistry Department and the Dean, Faculty of Science at Albaha University for laboratory facilities and encouragements.

Conflict of interest: The authors declare that no conflict of interest exists.

References

[1] Zabin SA, Abdelbaset M. Oxo/dioxo-vanadium(v) complexes with Schiff base ligands derived from 4-amino-5-mercapto-3-phenyl-1,2,4-triazole. Eur J Chem. 2016;7(3):322–8.

[2] Majid SA, Mir JM, Paul S, Akhter M, Parray H, Ayoub R, et al. Experimental and molecular topology-based biological implications of Schiff base complexes: a concise review. Rev Inorg Chem. 2019;39(2):113–28.

[3] da Silva CM, da Silva DL, Modolo LV, Alves RB, de Resende MA, Martins CV, et al. Schiff bases: a short review of their antimicrobial activities. J Adv Res. 2011;2(1):1–8.

[4] Chaturvedi D, Kamboj M. Role of Schiff base in drug discovery research. Chem Sci J. 2016;7(2):e114.

[5] Mallandur BK, Rangaiah G, Harohally NV. Synthesis and antimicrobial activity of Schiff bases derived from 2-chloro quinoline-3-carbaldehyde and its derivatives incorporating 7-methyl-2-propyl-3*H*-benzoimidazole-5-carboxylic acid hydrazide. Synth Commun. 2017;47(11):1065–70.

[6] Yernale NG, Mathada MBH. Synthesis, characterization, antimicrobial, DNA cleavage, and *in vitro* cytotoxic studies of some metal complexes of Schiff base ligand derived from thiazole and quinoline moiety. Bioinorg Chem Appl. 2014;2014:314963.

[7] Mistry BM, Kim DH, Jauhari S. Analysis of adsorption properties and corrosion inhibition of mild steel in

hydrochloric acid solution by synthesized quinoline Schiff base derivatives. Trans Indian Inst Met. 2016;69(6):1297–309.
[8] Salve PS, Alegaon SG, Srirram D. Three-component, one-pot synthesis of anthranilamide Schiff bases bearing 4-amino-quinoline moiety as *Mycobacterium tuberculosis* gyrase inhibitors. Bioorg Med Chem Lett. 2017;27:1859–66.
[9] Mandewale MC, Thorat B, Nivid Y, Jadhav R, Nagarsekar A, Yamgar R. Synthesis, structural studies and antituberculosis evaluation of new hydrazone derivatives of quinoline and their Zn(II) complexes. J Saudi Chem Soc. 2018;22: 218–28.
[10] Patil DY, Patil AA, Khadke NB, Borhade AV. Highly selective and sensitive colorimetric probe for Al^{3+} and Fe^{3+} metal ions based on 2-aminoquinolin-3-yl phenyl hydrazone Schiff base. Inorg Chim Acta. 2019;492:167–76.
[11] Hayat F, Salahuddin A, Umar S, Azam A. Synthesis, characterization, antiamoebic activity and cytotoxicity of novel series of pyrazoline derivatives bearing quinoline tail. Eur J Med Chem. 2010;45(10):4669–75.
[12] Boukabcha N, Djafri A, Megrouss Y, Tamer O, Avci D, Tuna M, et al. Synthesis, crystal structure, spectroscopic characterization and nonlinear optical properties of (*Z*)-*N*′-(2,4-dinitrobenzylidene)-2-(quinolin-8-yloxy)acetohydrazide. J Mol Struct. 2019;1194: 112–23.
[13] Ahmed M, Sharma R, Nagda DP, Jat JL, Talesara GL. Synthesis and antimicrobial activity of succinimido(2-aryl-4-oxo-3-{[(quinolin-8-yloxy)acetyl]amino}-1,3-thiazolidin-5-yl)acetates. ARKIVOC. 2006;11:66–75.
[14] Kavitha P, Saritha M, Reddy KL. Synthesis, structural characterization, fluorescence, antimicrobial, antioxidant and DNA cleavage studies of Cu(II) complexes of formyl chromone Schiff bases. Spectrochim Acta A Mol Biomol Spectrosc. 2013;102:159–68.
[15] Zabin SA. Antimicrobial, antiradical capacity and chemical analysis of *Conyza incana* essential oil extracted from aerial parts. J Essent Oil Bear Pl. 2018;21(2):502–10.
[16] Anand SAA, Loganathan C, Saravanan K, Alphonsa AJ, Kabilan S, Thomas NS. Synthesis, structure prediction, pharmacokinetic properties, molecular docking and antitumor activities of some novel thiazinone derivatives. N J Chem. 2015;39(9):7120–9.
[17] Feng X-Y, Jia W-Q, Liu X, Jing Z, Liu Y-Y, Xu W-R, et al. Identification of novel PPARα/γ dual agonists by pharmacophore screening, docking analysis, ADMET prediction and molecular dynamics simulations. Comput Biol Chem. 2019;78:178–89.
[18] Daina A, Michielin O, Zoete V. Swiss target prediction: updated data and new features for efficient prediction of protein targets of small molecules. Nucl Acids Res. 2019;47(W1):W357–64.
[19] Raj S, Sasidharan S, Dubey VK, Saudagar P. Identification of lead molecules against potential drug target protein MAPK4 from *L. donovani*: an *in silico* approach using docking, molecular dynamics and binding free energy calculation. PLoS One. 2019;14(8):e0221331.
[20] Zabin SA. Cu(II) and Ni(II) complexes derived from tridentate ligands with N=N and CH=N linkages: characterization and antimicrobial activity. Albaha Univ J Basic Appl Sci. 2017;1(2):9–18.
[21] Mandewale MC, Thorat B, Shelke D, Yamgar R. Synthesis and biological evaluation of new hydrazone derivatives of quinoline and their Cu(II) and Zn(II) complexes against *Mycobacterium tuberculosis*. Bioinorg Chem Appl. 2015;2015:153015.
[22] Saghatforoush LA, Chalabian F, Aminkhani A, Karimnezhad G, Ershad S. Synthesis, spectroscopic characterization and antibacterial activity of new cobalt(II) complexes of unsymmetrical tetradentate (OSN2) Schiff base ligands. Eur J Med Chem. 2009;44:4490–5.
[23] Bharadwaj SS, Poojary B, Kumar SM, Byrappa K, Nagananda GS, Chaitanya AK, et al. Design, synthesis and pharmacological studies of some new quinoline Schiff bases and 2,5-(disubstituted-[1,3,4])-oxadiazoles. N J Chem. 2017;41(16):8568–85.
[24] Paciorek P, Szklarzewicz J, Jasinska A, Trzewik B, Nitek W, Hodorowicz M. Synthesis, structural characterization and spectroscopy studies of new oxovanadium(IV,V) complexes with hydrazone ligands. Polyhedron. 2015;87:226–32.
[25] Al-Shaalan NH. Synthesis, characterization and biological activities of Cu(II), Co(II), Mn(II), Fe(II), and UO_2(VI) complexes with a new Schiff base hydrazone: *o*-hydroxyacetophenone-7-chloro-4-quinoline hydrazine. Molecules. 2011;16:8629–45.
[26] Rudbari HA, Iravani MR, Moazam V, Askari B, Khorshidifard M, Habibi N, et al. Synthesis, characterization, X-ray crystal structures and antibacterial activities of Schiff base ligands derived from allylamine and their vanadium(IV), cobalt(III), nickel(II), copper(II), zinc(II) and palladium(II) complexes. J Mol Struct. 2016;1125:113–20.
[27] Orojloo M, Zolgharnein P, Solimannejad M, Amani S. Synthesis and characterization of cobalt(II), nickel(II), copper (II) and zinc(II) complexes derived from two Schiff base ligands: spectroscopic, thermal, magnetic moment, electrochemical and antimicrobial studies. Inorg Chim Acta. 2017;467:227–37.
[28] Gup R, Kirkan B. Synthesis and spectroscopic studies of mixed-ligand and polymeric dinuclear transition metal complexes with bis-acylhydrazone tetradentate ligands and 1,10-phenanthroline. Spectrochim Acta A Mol Biomol Spectrosc. 2006;64:809–15.
[29] Shaghaghi Z. Spectroscopic properties of some new azo–azomethine ligands in the presence of Cu^{2+}, Pb^{2+}, Hg^{2+}, Co^{2+}, Ni^{2+}, Cd^{2+} and Zn^{2+} and their antioxidant activity. Spectrochim Acta A Mol Biomol Spectrosc. 2014;131:67–71.
[30] More G, Raut D, Aruna K, Bootwala S. Synthesis, spectroscopic characterization and antimicrobial activity evaluation of new tridentate Schiff bases and their Co(II) complexes. J Saudi Chem Soc. 2017;21:954–64.
[31] Alaghaz AMA, Ammar YA, Bayoumi HA, Aldhlmani SA. Synthesis, spectral characterization, thermal analysis, molecular modeling and antimicrobial activity of new potentially N_2O_2 azo-dye Schiff base complexes. J Mol Struct. 2014;1074:359–75.
[32] Mahal A, Abu-El-Halawa R, Zabin SA, Ibrahim M, Al-Refai M. Synthesis, characterization and antifungal activity of some metal complexes derived from quinoxaloylhydrazone. World J Org Chem. 2015;3(1):1–8.
[33] Shakdofa MME, El-Saied FA, Rasras AJ, Al-Hakimi AN. Transition metal complexes of a hydrazone–oxime ligand containing the isonicotinoyl moiety: Synthesis,

characterization and microbicide activities. Appl Organomet Chem. 2018;32(7):e4376.
[34] Ejidike IP, Ajibade PA. Synthesis, characterization, anticancer, and antioxidant studies of Ru(III) complexes of monobasic tridentate Schiff bases. Bioinorg Chem Appl. 2016;2016:9672451.
[35] Salehi M, Rahimifar F, Kubicki M, Asadi A. Structural, spectroscopic, electrochemical and antibacterial studies of some new nickel(II) Schiff base complexes. Inorg Chim Acta. 2016;443:28–35.
[36] Sonmez M. Synthesis and characterization of copper(II), nickel(II), cadmium(II), cobalt(II) and zinc(II) complexes with 2-benzoyl-3-hydroxy-1-naphthylamino-3-phenyl-2-propen-1-on. Turk J Chem. 2011;25:181–5.
[37] Das M, Chattopadhyay S. Designed synthesis of copper(II) and nickel(II) complexes with a tridentate N_2O donor Schiff base: Modulation of crystalline architectures through C–H···π and anion···π interactions. J Mol Struct. 2013;1051:250–8.
[38] Chah CK, Ravoof TBSA, Veerakumarasivam A. Synthesis, characterization and biological activities of Ru(III), Mo(V), Cd(II), Zn(II) and Cu(II) complexes containing a novel nitrogen-sulphur macrocyclic Schiff base derived from glyoxal. Pertanika J Sci Technol. 2018;26(2):653–70.
[39] Mahmoud WH, Mohamed GG, Elsawy HA, Mostafa A, Radwan MA. Metal complexes of novel Schiff base derived from the condensation of 2-quinoline carboxaldehyde and ambroxol drug with some transition metal ions. Appl Organomet Chem. 2018;32(7):e4392.
[40] Fonkui TY, Ikhile MI, Ndinteh DT, Njobeh PB. Microbial activity of some heterocyclic Schiff bases and metal complexes: a review. Trop J Pharm Res. 2018;17(12):2507–18.
[41] Alias M, Kassum H, Shakir C. Synthesis, physical characterization and biological evaluation of Schiff base M(II) complexes. J Assoc Arab Univ Basic Appl Sci. 2014;15:28–34.
[42] El-Sherif AA, Shoukry MM, Abd-Elgawad MMA. Synthesis, characterization, biological activity and equilibrium studies of metal(II) ion complexes with tridentate hydrazone ligand derived from hydralazine. Spectrochim Acta A Mol Biomol Spectrosc. 2012;98:307–21.
[43] Kramer SD, Wunderli-Allenspach H. Physicochemical properties in pharmacokinetic lead optimization. Farmaco. 2001;56(1–2):145–8.
[44] Neervannan S. Preclinical formulations for discovery and toxicology: Physicochemical challenges. Expert Opin Drug Metab Toxicol. 2006;2(5):715–31.
[45] Souza HDS, de Sousa PF, Lira BF, et al. Synthesis, in silico study and antimicrobial evaluation of new selenoglycolic-amides. J Braz Chem Soc. 2019;30(1):188–97.
[46] Ghose AK, Viswanadhan VN, Wendoloski JJ. A knowledge-based approach in designing combinatorial or medicinal chemistry libraries for drug discovery. 1. A qualitative and quantitative characterization of known drug databases. J Comb Chem. 1999;1(1):55–68.